ANEXO I

A COMPARATIVE STUDY BASED ON SIMULATIONS OF HEAT TRANSFERENCES ON HUMAN HEART, LIVER AND KIDNEY

Aguilar, J.[1], De la Fuente, I.[1], Salmerón, J.M. [2], Álvarez, S. [2], Risco R.[1]

[1]: CryoBioTech; Escuela Superior de Ingenieros, Universidad de Sevilla, 41092 Sevilla (España).

2: Departamento de Ingeniería Energética, Escuela Superior de Ingenieros, Universidad de Sevilla, 41092 Sevilla (España).

ABSTRACT

One main aim of cryopreservation is getting to have an everlasting organ bank. But yet a great improvement on technology and procedures is needed. In this context, the aim of this article is to present a comparative study on the temperature field variation of three human organs (the heart, the liver and the kidney). To achieve it a new software tool has been developed. This software can make simulations on the evolution of the temperature field of a selected organ tissue when perfused with a cryoprotector agent. This application solves the heat transference problem making use of a series of tools, such as the use of a digitally treated image of the tissue that is going to be studied. Another one is the use of a technique known as sub-structuring in order to get a much more accurate mathematical solution. After the simulation, the application gives us back the temperature obtained in each part of the studied section across all the time the

simulation lasted. The results obtained of the studied cases show that temperature field evolution depends directly on blood vessels. A larger number of these imply a fastest cooling velocity, as well as a more uniform special distribution. This produces a more homogeneous cooling process.

Key Words: organ preservation, perfusion, temperature field, digital image treatment

INTRODUCTION

Our main interest is tissue and organ cryopreservation. For this reason, a good knowledge of the temperature and cryoprotector concentration fields is necessary, not only to guarantee that at any place and at any time the concentration of cryoprotectant is high enough to avoid ice formation at a given temperature, but also in order to contend with dehydration. In conventional cryopreservation, dehydration is frequently of great importance for practical purposes: a reduction in the amount of water implies a reduction in the potential amount of ice, and also a depression of the melting point as a collateral effect. Prior knowledge of the transient temperature field is required to contend with dehydration. Finally, this requirement becomes even more evident in the case of vitrification.

Several attempts at computing the temperature field of perfused biological samples have been published in the past. A general analytical theory was set out by Klinger [13]. The use of Pennes' [12] and Weinbaum-Jiji's [14] bio-heat transfer equations and their interesting generalizations allowed the calculation of the average temperature field. A new approach was afforded by the use of statistical models [05]

which provided information on the most probable temperature. With the development of computers, these analytical and statistical methods have been replaced by numerical solutions. However, there are four important limitations to these approaches:

i) in some cases they do not deal with the transient [16,17];

ii) some of them only study a 1D situation [18, 19];

iii) perfusion through the vascular system is not taken into consideration [18]

iv) the geometries used are not real, but are, in every case, just approximations that have been generated in different ways.

In this article it is presented the development and functioning of a new tool, called ***Cryojab***, which pretends to cover all these limitations. Its basic grounds are the method of finite elements, sub-structuring and digital image treatment.

This document's structure is as follows: in the section entitled "Basic assumptions" the basis that the tool uses to create the simulations. In order to solve the mathematical problem in an efficient way, it is used the technique denominated as sub-structuring. This technique and its functioning are described in the section entitled "Sub-structuring". In the section entitled "Representation of the Space State Problem" is described the mathematical development in which the application is based. In the section entitled: "Functioning of the tool" the process to solve the problem is explained. Subsequently, the tool is used to carry out a series of simulations with sections extracted from three different organs: heart, kidney and liver, shown in the section entitled: "The simulations and their results". Finally in "Discussion" the conclusions achieved about the application developed and the results obtained of the simulations carried out by it are explained.

BASIC ASSUMPTIONS

1. **Geometry**. The tool works in 2D geometry because it uses a digital image of the tissue to study as input for simulating the transient of the temperature. The results of the simulations show temperature maps based on the input image.
2. **Organs' behaviour**. The application carries out a simulation of a perfusion o fan organ through its vascular system. But the offered results have been calculated only for the section that appears in the photograph used as input.
3. **Conduction vs. Convection**. When an organ is cooled through its vascular system, convection is the predominant method of heat transfer in the large vessels [20, 21]. However, here we are dealing not with the situation in the large vessels, but in the capillaries. In these, the cooling agent flows very slowly (for a physiological regime) and the heat transfer mechanism can be accurately approximated by conduction. Naturally, for the whole issue to be dealt with (large, intermediate and small vessels) conduction must be complemented with convection.
4. **The physical properties of the materials (density, thermal conductivity and calorific capacity) do not vary across the time**. The mechanisms that produce modification on these parameters are temperature field variation and a change on the stage of the materials. On the one hand, the rank of the studied values for the temperature is little enough to consider it as constant. So it will be supposed that there won't exist a change on the stage of the materials.
5. **No mass transfer during the process**. In our case we are assuming that there is no ice formation, which is one of the most important mechanisms of mass transfer. The second mass transfer mechanism is the required diffusion of the cryoprotectant agent, an essential ingredient of almost any cryopreservation protocol. However,

for the sake of simplicity we shall assume a non permeable isosmotic cooling agent is used that does not change mass distribution in the perfused organ.

SUB-STRUCTURING

It has been said that the image studied with this application contains different types of materials. This provides the organ of some heterogeneity and certain thermal inertia. This in addition to the fact that the organ is frozen progressively produces a transient conduction regimen. Therefore it requires a procedure that provides us with a fast and versatile simulation though by the way it would be less accurate.

The key to solve this resides in sub-structuring. The image is divided into different sub-structures (which at the time are divided in nodes corresponding to each pixel of the image) that are modelled individually, establishing subsequently the constraints between the degrees of freedom of each sub-structure [15]. As a result, it is possible to divide the system into several sub-zones linked in one way or another to the others.

The main advantage of using the sub-structuring procedure is that it saves computational time as a consequence of using dimensionally smaller matrices: it is easier to invert several matrices of small dimension than a single matrix composed of all of these. Nevertheless, these procedures have some drawbacks. For example, our decision to avoid the assessment of the whole system in one step means that its eigenvalues cannot be obtained directly. If this additional information is needed, the traditional approach must be used. This is not our case because we are not solving the problem using transfer functions but finite differences. There are several ways to

accomplish the link-up. The best strategies as far as the present work is concerned are those that use the temperature in the adjacent nodes as the link-up variable. We shall use an iterative sub-structuring method with coupling through equivalent temperature. Using an initial solution for the temperature field as our starting point, we find solutions for all the sub-structures one by one; when a solution is found for a sub-structure, its temperature field in the proximities of another sub-structure will be used to find a solution for the next sub-structure.

The sub-structure could have homogeneous or heterogeneous properties depending on the number of elements present. Our tool only realizes simulations with homogeneous substructures. The sequence in which the sub-structures are solved can be altered in order to improve convergence by accelerating the propagation of the boundary conditions across the entire structure. In the complex case of multidimensional conduction it is necessary to generalise the process. An isotropic order of resolution without preferential sub-structures has been chosen.

The foregoing method achieves node by node coupling between sub-structures. This approach proves to have a major limitation. If an element has to be represented by two adjacent sub-structures, then their respective nodes cannot be properly aligned. To overcome this problem, interpolation was used to establish a linear approximation between the temperatures of two nodes in the same sub-structure and the corresponding temperature of the opposite node in this line was then calculated.

REPRESENTATION OF THE PROBLEM IN THE SPACE STATE

The Conduction Transfer Function (CTF) reduces the second order differential Fourier conduction heat equation to a set of linear algebraic equations. There are two approaches to solve the CTF coefficients required for applying the CTF method: the Laplace Transform method and the Space State method. The Laplace Transform is the traditional method to calculate CTF. Although it requires more CTF coefficients than the Laplace approach, three major advantages are offered by the Space State method. Firstly, its mathematical sequence has a more straightforward interpretation as the need for complex functions is eliminated. Secondly, the Space State Method allows solutions for CTF coefficients to be obtained with shorter time lapses. And thirdly, the Space State Method has been shown to be more accurate than the Laplace or analytical techniques.

If the Space State formalism is provided with a grid, the heat transfer problem is represented by the following set of equations:

$$\{\dot{T}_n\} = [A]\{T_n\} + [B]\{T_{cc}\} + [I]\{G\} = [A]\{T_n\} + [B](\{T_{cc}\} + \{G'\}) \quad (1)$$

$$\{Q_{cc}\} = [C]\{T_n\} + [D]\{T_{cc}\} \quad (2)$$

$$\{T_n(0)\} = \{T_{n0}\} \quad (3)$$

where $\{T_n\}$ is the vector of temperatures (its elements are the temperature in each of the elements of the grid), $\{T_{cc}\}$ is the vector of the contour conditions, $\{T_{n0}\}$ is the vector for the initial conditions and $\{G\}$ is the vector of the heat (cold, in this case) generation. $[I]$ is the identity matrix, and $[A]$, $[B]$, $[C]$ and $[D]$ are the matrices for the internal description of the system; these are all computed below.

As is usually the case, the first order linear differential equations 1-3 are solved by breaking them down into homogeneous and non-homogeneous problems. The solution to the complete problem is obtained by adding the general solution of the homogeneous system to a particular solution of the non-homogeneous system. To solve the homogeneous problem we perform a change of base (to a diagonal matrix) and then integrate. By applying Duhamel's integral [11] and assuming a linear evolution of the temperature in the contour during the time interval [t, t+Δt] (the values of the temperature at t and t+Δt are obviously known from the chosen cooling rate), the solution of the non-homogeneous system is given by:

$$\begin{aligned}\{T_n(t+\Delta t)\} &= [P]\left[e^{l(i)\cdot(\Delta t)}\right][P]^{-1}\{T_n(t)\}+[P][E][P]^{-1}[B]\{T_{cc}(t)\}+\\ &+[P][F][P]^{-1}[B]\{T_{cc}(t+\Delta t)\}+[P][H][P]^{-1}[B]\{G'\};\ \ 0<i<nn-1\end{aligned} \tag{4}$$

here $l(i)$ are the elements of a diagonal matrix composed of the eigenvalues of the matrix $[A]$, and $[P]$ is the change of base matrix. The diagonal matrixes $[E]$, $[F]$ and $[H]$ depend on the eigenvalues and on the time step, and are given by:

$$e(i)=\left(\int_0^{\Delta t}\left[e^{l(i)\cdot(\Delta t-\tau)}\right]\left(1-\frac{\tau}{\Delta t}\right)d\tau\right)=\frac{l(i)\cdot\Delta t\cdot e^{l(i)\cdot\Delta t}+1-e^{l(i)\cdot\Delta t}}{l(i)^2\cdot\Delta t} \tag{5}$$

$$f(i)=\left(\int_0^{\Delta t}\left[e^{l(i)\cdot(\Delta t-\tau)}\right]\left(\frac{\tau}{\Delta t}\right)d\tau\right)=\frac{-l(i)\cdot\Delta t-1+e^{l(i)\cdot\Delta t\cdot}}{l(i)^2\cdot\Delta t} \tag{6}$$

$$h(i)=\left(\int_0^{\Delta t}\left[e^{l(i)\cdot(\Delta t-\tau)}\right]d\tau\right)=\frac{e^{l(i)\cdot\Delta t}-1}{l(i)};\ 0<i<nn-1 \tag{7}$$

Meanwhile, from the equation that relates the outputs to the inputs and the state variables vector, Eq. (2), we find:

$$Q_{cc}(t+\Delta t)=\{VP(t)\}+[MA]\cdot\{T_{cc}(t+\Delta t)\} \tag{8}$$

were

$$\begin{aligned}\{VP(t)\} &= [C][P]\left[e^{J(i)\cdot(\Delta t)}\right][P]^{-1}\{T_n(t)\}+ \\ &+ [C][P][E][P]^{-1}[B]\{T_{cc}(t)\}+[C][P][H][P]^{-1}\{G\}\end{aligned} \tag{9}$$

and

$$[MA] = [C][P][F][P]^{-1} + [D] \tag{10}$$

Eq. (8) will be used to solve the thermal coupling with other elements, relating the heat flow across the boundaries of the element to its surface temperatures. This heat flow, at any given instant, will depend on two constituents: one is the "principal vector" $\{VP\}$, which contains information about the state vector and excitation during the preceding instant; this vector therefore changes with time. The other is the product of a coupling matrix, $[MA]$, and the excitation temperatures at that very instant. The matrix $[MA]$ contains information about the dynamics of the system, provided by the properties of the material and its geometry. If these remain constant over time, the system eigenvalues and the system matrix will also remain constant. With Equations (4) and (8) numerical and computer implementation is performed iteratively. So the resolution of system of first-order linear differential equations (Equations 1-3) is:

$$\{T_i(t+\Delta t)\} = [P]\left[e^{J(i)\cdot(\Delta t)}\right][P]^{-1}\{T_i(t)\}+[P]\int_0^{\Delta t}\left[e^{J(i)(\Delta t-\tau)}\right][P]^{-1}[B]\left\{\{T_{ic}(t)\}+\frac{\{T_{ic}(t+\Delta t)\}-\{T_{ic}(t)\}}{\Delta t}\tau+\{G\}\right\}d\tau \tag{11}$$

and

$$\begin{aligned}\{Q_{ic}(t+\Delta t)\} &= [C][P]\left[e^{J(i)\cdot(\Delta t)}\right][P]^{-1}\{T_i(t)\}+[C][P][E][P]^{-1}[B]\{T_{ic}(t)\}+ \\ &+ [C][P][H][P]^{-1}\{G\}+\left[[C][P][F][P]^{-1}+[D]\right]\{T_{ic}(t+\Delta t)\},\end{aligned} \tag{12}$$

with the initial conditions

$$\{T_i(t=0)\} = \{T_{i0}\} \tag{13}$$

where $l(i)$ are the elements of a diagonal matrix composed of the eigenvalues of $[A]$. The auxiliary matrixes $[E]$, $[H]$, $[P]$ and $[F]$ are described in the appendix. The matrices $[A]$ and $[B]$ are obtained by comparing Eq. 1 with Fourier's equation in two dimensions,

$$\frac{\partial^2 T}{\partial x^2}+\frac{\partial^2 T}{\partial y^2}=\frac{1}{\alpha}\frac{\partial T}{\partial t} \tag{14}$$

written in a discrete way.

In the following we shall use the symbol $\mu=\rho c_p$ for short. In order to write Eq. (14) in a discrete way it is necessary to select a specific grid on the tissue. Different schemes can be used to achieve this: finite differences, finite elements or finite volumes. As our geometry can easily be represented by Cartesian coordinates, the accuracy provided by finite differences is sufficiently great. Additionally, a finite differences' scheme is simpler to implement than one of finite elements or finite volumes; therefore, this approach will be taken. We shall divide the tissue into *nx* times *ny* squares, usually called "nodes" in Space State method literature, labelled with the symbol (*i*,*j*). So, $k_{i,j}$, $\mu_{i,j}$, $dx_{i,j}$ and $dy_{i,j}$ represent thermal conductivity, density times, specific heat and the dimensions of the node (*i*,*j*) respectively. From the Eq. (14):

$$\frac{dT_{i,j}}{dt}=\frac{1}{\mu_{i,j}dx_{i,j}}\cdot\left(\frac{T_{i-1,j}-T_{i,j}}{\frac{dx_{i-1,j}}{2k_{i-1,j}}+\frac{dx_{i,j}}{2k_{i,j}}}+\frac{T_{i+1,j}-T_{i,j}}{\frac{dx_{i+1,j}}{2k_{i+1,j}}+\frac{dx_{i,j}}{2k_{i,j}}}\right)+\frac{1}{\mu_{i,j}dy_{i,j}}\cdot\left(\frac{T_{i,j-1}-T_{i,j}}{\frac{dy_{i,j-1}}{2k_{i,j-1}}+\frac{dy_{i,j}}{2k_{i,j}}}+\frac{T_{i,j+1}-T_{i,j}}{\frac{dy_{i,j+1}}{2k_{i,j+1}}+\frac{dy_{i,j}}{2k_{i,j}}}\right) \tag{15}$$

By comparing Eq. (15) with Eq. (1) it is possible to obtain all the elements of the matrix $[A]$. The right hand side of Eq. (15) contains eight terms. The four indices of the terms labelled *i, j* coincide with the index of the time derivative on the left hand side.

Therefore these four terms form the diagonal elements of the matrix $[A]$. The rest of the terms, identified by their indices, correspond to the other elements around the node. The remaining elements of $[A]$ are zero. Therefore we arrive at:

Main diagonal:

$$a(j+nyi,\, j+nyi) = -\frac{1}{\mu_{i,j}dy_{i,j}}\cdot\left[\frac{2}{\frac{dy_{i,j-1}}{k_{i,j-1}}+\frac{dy_{i,j}}{k_{i,j}}}\right]-\frac{1}{\mu_{i,j}dy_{i,j}}\cdot\left[\frac{2}{\frac{dy_{i,j+1}}{k_{i,j+1}}+\frac{dy_{i,j}}{k_{i,j}}}\right]$$
$$-\frac{1}{\mu_{i,j}dx_{i,j}}\cdot\left[\frac{2}{\frac{dy_{i-1,j}}{k_{i-1,j}}+\frac{dy_{i,j}}{k_{i,j}}}\right]-\frac{1}{\mu_{i,j}dx_{i,j}}\cdot\left[\frac{2}{\frac{dy_{i+1,j}}{k_{i+1,j}}+\frac{dy_{i,j}}{k_{i,j}}}\right];\quad 0\le j\le ny-1 \tag{16}$$

The other elements that are not zero are:

$$a(j+ny\cdot i,\,(j-1)+ny\cdot i) = \frac{1}{\mu_{i,j}dy_{i,j}}\cdot\left[\frac{2}{\frac{dy_{i,j-1}}{k_{i,j-1}}+\frac{dy_{i,j}}{k_{i,j}}}\right];\quad j>0$$

$$a(j+ny\cdot i,\,(j+1)+ny\cdot i) = \frac{1}{\mu_{i,j}dy_{i,j}}\cdot\left[\frac{2}{\frac{dy_{i,j+1}}{k_{i,j+1}}+\frac{dy_{i,j}}{k_{i,j}}}\right];\quad j<ny-1$$

$$a(j+ny\cdot i,\, j+ny\cdot(i-1)) = \frac{1}{\mu_{i,j}dx_{i,j}}\cdot\left[\frac{2}{\frac{dy_{i-1,j}}{k_{i-1,j}}+\frac{dy_{i,j}}{k_{i,j}}}\right];\quad i>0 \tag{17}$$

$$a(j+ny\cdot i,\, j+ny\cdot(i+1)) = \frac{1}{\mu_{i,j}dx_{i,j}}\cdot\left[\frac{2}{\frac{dy_{i+1,j}}{k_{i+1,j}}+\frac{dy_{i,j}}{k_{i,j}}}\right];\quad i<nx-1$$

The elements of the matrix $[B]$ can be calculated in a similar way. In this case, reference should be made to the conditions at the boundary. For example, for the right edge these are:

$$\frac{\partial T_{i,j}}{\partial t}=\frac{1}{\mu_{i,j}dx_{i,j}}\left(\frac{T_{i-1,j}-T_{i,j}}{\frac{dx_{i-1,j}}{2k_{i-1,j}}+\frac{dx_{i,j}}{2k_{i,j}}}+\frac{T_{cc}-T_{i,j}}{R_{cc}+\frac{dx_{i,j}}{2k_{i,j}}}\right)+\frac{1}{\mu_{i,j}dy_{i,j}}\left(\frac{T_{i,j-1}-T_{i,j}}{\frac{dy_{i,j-1}}{2k_{i,j-1}}+\frac{dy_{i,j}}{2k_{i,j}}}+\frac{T_{i,j+1}-T_{i,j}}{\frac{dy_{i,j+1}}{2k_{i,j+1}}+\frac{dy_{i,j}}{2k_{i,j}}}\right) \tag{18}$$

where R_{cc} is the boundary resistance. The elements of the matrix $[B]$ can be obtained from this. Non-zero elements are:

$$\begin{aligned}
&b(ny\cdot i,i)=\frac{1}{\mu_{i,0}dx_{i,0}}\cdot\left[\frac{2}{R_{cc,i}+\frac{dx_{i,0}}{k_{i,0}}}\right];\quad 0\le j\le ny-1\\
&b(ny-1+ny\cdot i,i+nx)=\frac{1}{\mu_{i,ny-1}dx_{i,ny-1}}\cdot\left[\frac{2}{R_{cc,i+nx}+\frac{dx_{i,ny-1}}{k_{i,ny-1}}}\right];\quad 0\le j\le ny-1\\
&b(j,2\cdot nx+j)=\frac{1}{\mu_{0,j}dx_{0,j}}\cdot\left[\frac{2}{R_{cc,2nx+j}+\frac{dx_{0,j}}{k_{0,j}}}\right];\quad 0\le j\le ny-1\\
&b(j+ny\cdot nx-ny,2\cdot nx+ny+j)=\frac{1}{\mu_{nx-1,j}dx_{nx-1,j}}\cdot\left[\frac{2}{R_{cc,2nx+ny+j}+\frac{dx_{nx-1,j}}{k_{nx-1,j}}}\right];\quad 0\le j\le ny-1
\end{aligned} \tag{19}$$

A parallel analysis gives us the matrices that relate the heat flows with the nodal and boundary temperatures, $[C]$ and $[D]$ respectively. To this end we have to write the heat equation in a discrete way:

$$Q_{cc}(i,j) = 2k_{i,j}\frac{T_n(i,j) - T_{cc}(i,j)}{dx_{i,j}dy_{i,j}} \tag{22}$$

By direct comparison of Eq. (22) with Eq. (2) we arrive at:

$$\begin{aligned}
&c(i, ny\cdot i) = \frac{2k_{i,0}dx_{i,0}}{dy_{i,0}}; \quad 0 \le j \le ny-1 \\
&c(i+nx, ny-1+ny\cdot i) = \frac{2k_{i,ny-1}dx_{i,ny-1}}{dy_{i,ny-1}}; \quad 0 \le j \le ny-1 \\
&c(2\cdot nx+j, j) = \frac{2k_{0,j}dy_{0,j}}{dx_{0,j}}; \quad 0 \le j \le ny-1 \\
&c(2\cdot nx+ny+j, j+ny\cdot nx-ny) = \frac{2k_{nx-1,j}dy_{nx-1,j}}{dx_{nx-1,j}}; \quad 0 \le j \le ny-1
\end{aligned} \tag{23}$$

$$\begin{aligned}
&d(i) = \frac{2k_{nyi}dx_{nyi}dz}{dy_{nyi}}; \quad 0 \le i \le nx \\
&d(i+nx) = \frac{2k_{ny(i+1)-1}dx_{ny(i+1)}dz}{dy_{nyi}}; \quad 0 \le i \le nx \\
&d(i+2nx) = \frac{2k_i dy_i dz}{dx_i}; \quad 0 \le i \le ny \\
&d(i+2nx+ny) = \frac{2k_{i+nn-ny}dy_{i+nn-ny}}{dx_{i+nn-ny}}; \quad 0 \le i \le ny
\end{aligned} \tag{24}$$

APPLICATION OPERATION

The application ***Cryojab*** has a two stage functioning. On the one hand, an interface designed to introduce the data corresponding to the simulation and to present the results. On the other hand, a subroutine that carries out the whole mathematical calculation with the data already introduced. The interface is implemented in PHP, while the subroutine is implemented in C++. Tasking all this into account, the minimum

requisite for the tool to function correctly is a Pentium III equipment with 128 MB of RAM.

The process to carry out the simulation is the following one: first of all, the user is required to introduce the image of the tissue that is going to be studied. This image is divided into grids. For this reason the image resolution influences directly in the number of sustructuring. The number of sustructuring and the size of them influence directly in the time of processing. Because of this, it is offered the possibility of reducing the image's size. Through it, it is reached an agreement between the precision and rapidity in the simulation.

The image has a tincture in order to identify the different materials. In the next step the colours to distinguish the different materials present in the image are selected. Then the application makes a new sampling of the image, offering a new image with the detected colours. This is the image that is going to be used throughout the rest of the process.

Next there is a request of the proper parameters for the simulation, it is, physical properties of the materials (these being identified with the selected colours), properties of the cryoprotector agent, conditions of the image surrounding (which can be adiabatics or of a fixed temperature by means of a lineal function) and the period of time during which the simulation is going to be carried out.

When all the parameters have been introduced, the mathematical calculation starts. The interval of time to simulate and the image resolution are two factors determining the time needed to complete the simulation. As higher is the simulated

interval and higher resolution of the image, more time would be needed to complete this process.

Once that all the information has been processed a results screen is shown. In it, all the numerical results of the whole interval or of a determined moment can be consulted. In this last case, it is offered the possibility of showing graphically the results through a little code of Matlab®.

THE SIMULATIONS AND ITS RESULTS

Nine different simulations have been prepared: three organs (heart, kidney and liver) and three different cooling velocities (-0,2, -0,4 y -0,8 ºC/s). The bigger part of parameters is fixed for all the simulations (only, physical properties of the materials do vary). The sections selected as representatives are: the cardiac muscle related to the heart (figure 2.a), the hepatic gland related to the liver (figure 2.b) and the renal cortex related to the kidney (figure 2.c). The images shown in figure 2 have been digitally retouched in order to produce an effective identification of the different materials. The real size of the sections contained in the images is of 140.5 µm. x 187.5 µm. The images have been resized to a 60x80 pixels resolution to achieve an equilibrium between precision and velocity in the calculation of the simulation. The initial temperature of the organs is 36º C. The contour conditions are adiabatic for the four sides of the image, it's to say, symmetric conditions. The cryoprotector agent has an initial temperature of 36º C. The simulation time interval depends of the cooling rate. For -0,2º C/s would be of 240 s. For -0,4º C/s would be of 120 s. And to finish, for -0,8º C/s would be of 60 s.

As a simulation sample, it is offered the images given back by the application for the moment 60 s. of the three organs for a cooling rate of -0,2º C/s (Figure 3). More moments of the initial stage of the simulation have been selected as it is where a more variable behaviour has been registered. Making use of the average and the typical deviation of the temperature in these moments of time a series of tables and graphics are extracted.

The temporal evolution of the average temperature is shown in Figure 4. Figure 5 shows the temporal evolution of the slope of the average temperature. Table 2 contains the numerical data of the average temperature in the selected moments of time. Table 3 contains the numerical data of the slope of standard deviation in the selected moments of time.

Taking into accounts these data it is observed that the variation of the average temperature of the organ presents some thermal inertial at the beginning of the simulation. Nevertheless, it is observed that the duration of this inertia does not mainly depend on the cooling rate. For the three cooling rates studied, the transient approximately lasts 40 s. Once that this inertial stage has been finished, a lineal regime of the temperature variation is achieved. The data about the slope show that it tends to establish itself as time passes. Once reached the stationary regime, the differences among the average temperature of the studied sections are almost constant. Compare the temperature evolution of the studied sections, it is shown that the one of kidney has a faster evolution than the ones of heart and liver. The last ones present a similar evolution. It is also observed that when the cooling rate is higher, more differences appear among the different organs.

The temporal evolution of the standard deviation of temperature is shown in figure 6. Figure 7 shows the slope of standard deviation of temperature across time. Table 4 contains the numerical data of the standard deviation for every simulation. Table 5 contains the numerical data of the slope of the standard deviation of temperature.

The data show that the standard deviation grows considerably in the moments that the organ possesses the thermal inertia previously mentioned. Once that this stage has been finished the standard deviation tends to maintain constant. It can be checked observing the slope graphics. It is observed an important increase on the first moments that will descend rapidly. Next it is shown an inflection point, after which it would finally descend softly. This behaviour its common to the three groups of simulations, and independently of the cooling rate, it occurs at the time moments of time. However, the differences among the average temperature of the organs grow at the same time that the cooling rate increases.

DISCUSSION

Currently, transplantation is the only solution for patients suffering from organ failure at advanced stages. As a result of this, organ banking will provide medicine with a very powerful tool. It is important, however, to note that there have been few successful reports on organ cryopreservation, and even less with a greater success rate than the one achieved by the work of A.U. Smith [22] in 1961. None of these were related to organs that require the complete recovery of a complex vascular system.

A strong understanding of the temperature field during cooling process is crucial for the design of a cryopreservation protocol that prevents ice formation, which is probably the only valid approach to the problem. Several models have been published to compute this temperature field in the past. In these models the authors have been able to tackle very important issues that our model, in its present form, does not. It is important to note however, that these models leave significant gaps in the understanding of these temperature fields that this new tool will help to fill.

It has been presented a novelty tool that allows people to get to an approximate behaviour of a tissue belonging to an organ cool though perfusion of a cryoprotector agent. The morphological information of the organ is introduced in the application by an image of a tissue belonging to a section of the organ. This providing the tool of a high rate of versatility. Taking this image as an initial point the tool solves the problem of heat transference very efficiently thanks to the application of the finite element method and substructuring.

Making use of the application nine different simulations have been carried out. From these it have been extracted a series results and conclusions. Taking into account that the simulations with the same cooling rate share almost all parameters, and that those that differ are practically equal, it can be guessed that the more notably influential parameter over the results if the image of the tissue used as starting point for each simulation. It is to say, the morphology of each tissue.

Observing the data related to the average temperature, it is established that the kidney is the organ that cools more rapidly. In contrast it has been found out that heart and liver show a slower evolution. If the three images are compared it can be concluded that the kidney have much more capillary vessels than liver and heart. So, as a

conclusion it can be set that the parameter that influences more directly on the cooling rate of an organ is the number of capillary vessels that it has.

Observing now the data related to the standard deviation of temperature, it is extracted that the kidney is the organ that more regularly is cooled while the heart and liver do in a less homogeneous way. It is also observed that the kidney presents a much more homogeneous distribution of capillary vessels than the other two organs mentioned before. This can be appreciated clearly in Figure 3. Thus it can be achieved the conclusion that homogeneity on the variation of the temperature inside an organ depends directly on the physical distribution of the capillary vessels of it. As more uniform is the distribution, lesser is the standard deviation, and because of this the organ cools more regularly.

Finally the simulations are compared varying the cooling rate. The first important data extracted is that doubling the cooling rate does not suppose dividing in two the simulation interval. The average temperature reached is higher when the cooling rate is higher as well. Thus for a cooling rate of -0,8º C/s after 240 s. we get an average temperature of approximately -8º C. On the other hand, for a cooling rate of -4º C/s after 120 s. we get an average temperature of approximately -5º C. As well as for a cooling rate of -0,2º C/s after 60 s. we get an average temperature of approximately 1º C. Nevertheless, the different stages occur approximately at the same moments of time.

In this way, it can be reach the conclusion that the temperature variation inside an organ depends mainly on its morphology. Apart from it, the behaviour that organs present is maintained at the same temporal moments, independently of the cooling rate velocity.

REFERENCES

[1] Palsson, B., Hubbell, J.A., Plonsey, R., Bronzino, J.D., "Tissue Engineering", CRC Press, Boca Raton, FL, 2000, pp. 20-1 - 20-9, 24-1 – 24-17.

[2] Lanza, R.P., Langer, R., Vacanti, J., "Principles of Tissue Engineering (Second Edition)", Academic Press, San Diego, 2000, pp. 541-550, 645-652.

[3] Latarjet, M., Ruiz-Liard, A., "Anatomía Humana, Tomo 2 (4ª Ed.)", Editorial Medica Panamericana, Buenos Aires, 2006, pp. 1376-1400, 1510-1526.

[4] Ross, M.H., Kaye, G.I., Paulina, W., "Histología, Texto y Atlas color con biología celular y molecular (4ª Ed.)", Editorial Medica Panamericana, Buenos Aires, 2006, pp. 264-266, 345-347, 534-540, 606-615.

[5] Valvano, J.W., "Bioheat transfer", Biomedical Engineering Program, Department of Electrical and Computer Engineering, The University of Texas, Austin, pp. 14-19.

[6] Chato, J.C., Lee, R.C., "The Future of Biothermal Engineering", Bioengineering Faculty and the Department of Mechanical and Industrial Engineering, The University of Illinois, Urbana-Champaing. Holmes, K.H., "Appendix: Thermal Conductivity of Selected Tissues".

[7] Valvano, J.W., Cochran, J.R., Diller, K.R., "Thermal Conductivity and Diffusivity of Biomaterials Measured with Self-Heated Thermistors", International Journal of Thermophysics, Bélgica, 1985, pp. 308-310.

[8] Aguilar, J., "Estudio del campo de temperatura en el corazón aplicado a la conservación de órganos en frio", Universidad de Sevilla, Sevilla, 2003.

[9] Martín-Lacave, I., San Martín Díez, M.V., "Atlas practico de histología", Díaz de Santos, Madrid, 2005.

[10] Nagle, R.K., Saff, E.B., Snider, A.D. "Fundamentals of Differential Equations", Fifth Edition , Addison-Wesley, 2000.

[12] Pennes, H.H., "Analysis of Tissue and Arterial Blood in the Resting Human Forearm", Journal of Applied Physiology, 1, 93-22 (1948).

[13] Klinger H.G., "Heat Transfer in Perfused Biological Tissue-General Theory", Bull. Math. Bio. 36, 403-415 (1978).

[14] Weinbaum, S., Jiji, L.M., S "A New Simplified Bioheat Equation for the Effects of Blood Flow on Local Average Tissue Temperature", ASME Journal of Biomechanical Engineering 107, 131-139 (1985).

[15] Allen, M.B., Herrera, I., Pinder, G.F., "Numerical modelling in Science and Engineering", John Wiley and Sons, Ed. (1988).

[16] Blanchard, C.H., Gutierrez, G., White, J.A., Roemer, R.B., "Hybrid Finite Element-Finite Difference Method for Thermal Analysis of Blood Vessels", Int. J. Hyperthermia, 16, 341-353 (2000).

[17] Huang, H.W., Chen, Z.P., Roemer, R.B., "A Counter Current Vascular Network Model for Heat Transfer in Tissues", ASME Journal of Biomechanical Engineering, 118, 120-129 (1996).

[18] Cui, Z.F., Cui, R.C., Dykhuizen, R.C., Nerem, R.M., Sembanis, A., "Modeling of Cryopreservation of Engineered Tissues with One-Dimensional Geometry", Biotechnol. 18, 354-361 (2002).

[19] Zhang, Y.T., Liu, J., Y "Numerical study on three-region thawing problem during cryosurgical re-warming", Medical Engineering and Physics 24, 265-277 (2002).

[20] Rubinsky, B., "Heat transfer during cryopreservation", in "The Biophysics of Organ Cryopreservation", edit. D. E. Pegg and A.M. Karow Jr., Plenum Press, 1987.

[21] Rubinsky, B., "Heat transfer during cryopreservation by perfusion through the vascular system". Cryobiology 24, 537-541 (1987).

[22] Smith, A.U., "The effects of glycerol and freezing on mammalian organs", in: A.U. Smith (Ed.), "Biological Effects of Freezing and Supercooling", Edward Arnold, London, 1961, pp. 247-269.

NOMENCLATURE

Specific density:

c_ρ = specific heat (J/kg·ºC)

k = thermal conductivity (W/m·ºC)

α = thermal diffusivity ($W/J \cdot m^2$)

ρ = density (kg/m^3)

FIGURES

Figure 1: an organ section (picture taken from [9]). The method of finite differences and sub-structuring imposes two meshes on the picture. The fine mesh divides the sample

into nodes. The gross mesh divides the sample into sub-structures. Each sub-structure is solved independently of the others.

Figure 2: images digitally treated that will function as input for the system in the three study cases (a. heart, b. liver, c. kidney, taken from [9]).

Figure 3: temperature maps for each simulation returned by the tool on 60 s. (a. heart, b. liver, c. kidney).

Figure 4: graphic containing the temporal evolution of the average temperature inside the organ in each of the three organs studied (a. -0.2 °C/s., b. -0.4 °C/s, c. -0.8 °C/s).

Figure 5: graphic containing the temporal evolution of the standard deviation of the temperature inside the organ in each of the three organs studied (a. -0.2 °C/s., b. -0.4 °C/s, c. -0.8 °C/s).

Figure 6: graphic containing the temporal evolution of the slope of the average temperature inside the organ in each of the three organs studied (a. -0.2 °C/s., b. -0.4 °C/s, c. -0.8 °C/s).

Figure 7: graphic containing the temporal evolution of the slope of the standard desviation of the temperature inside the organ in each of the three organs studied (a. -0.2 °C/s., b. -0.4 °C/s, c. -0.8 °C/s).

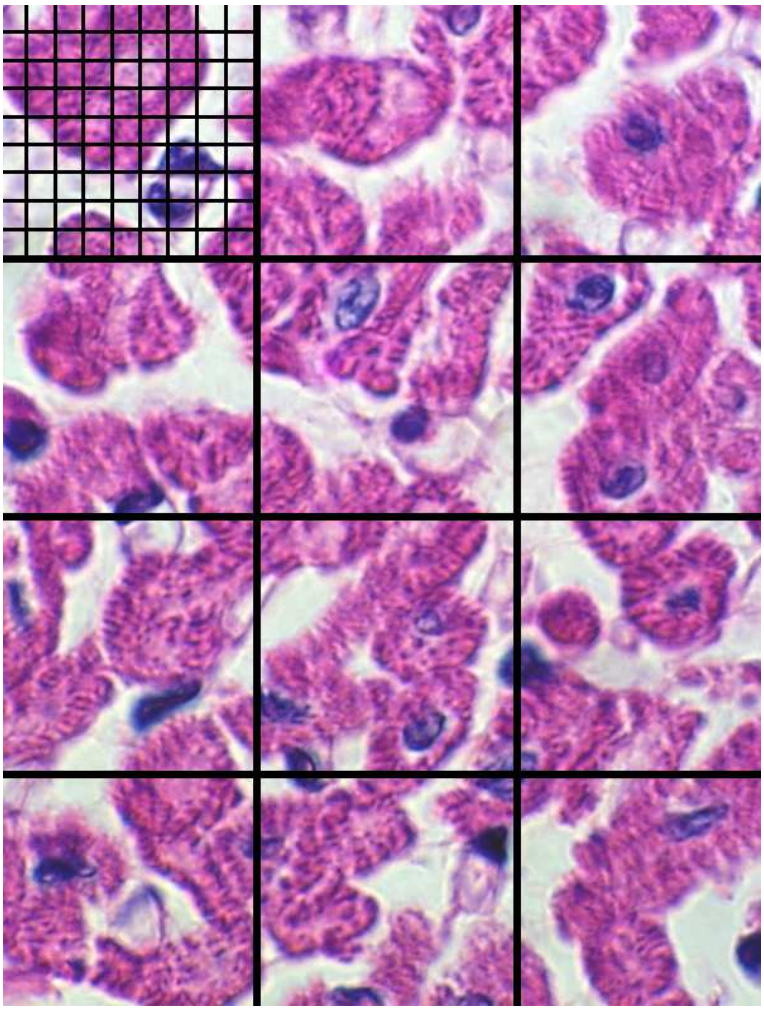

Figure 1

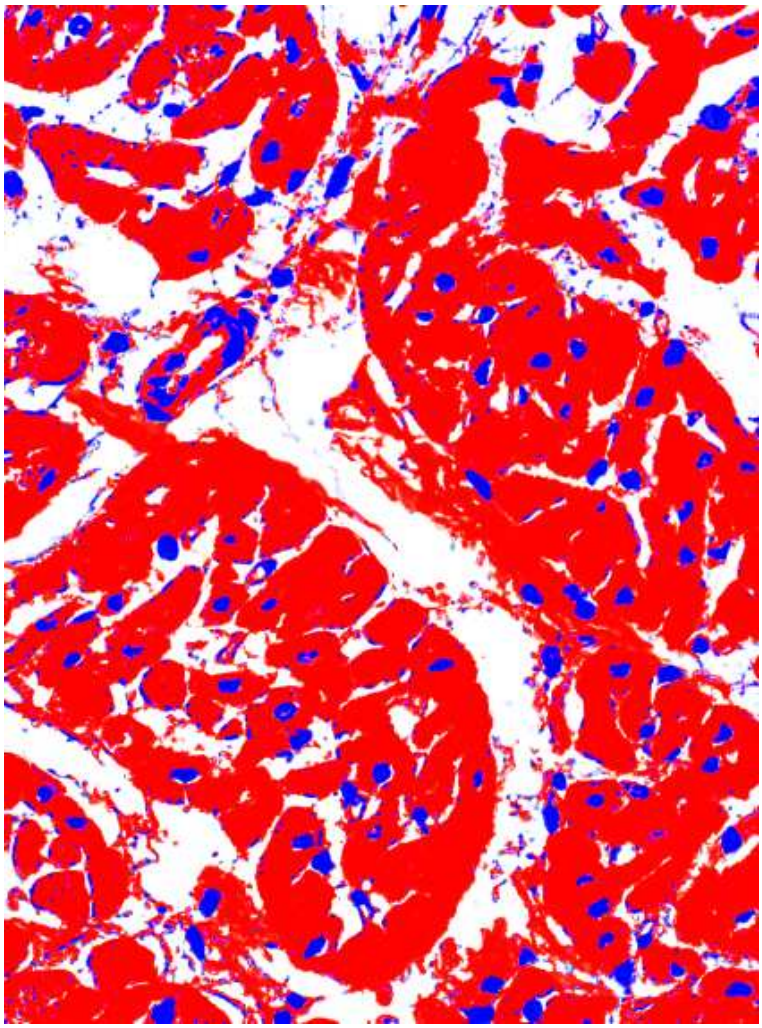

Figure 2.a

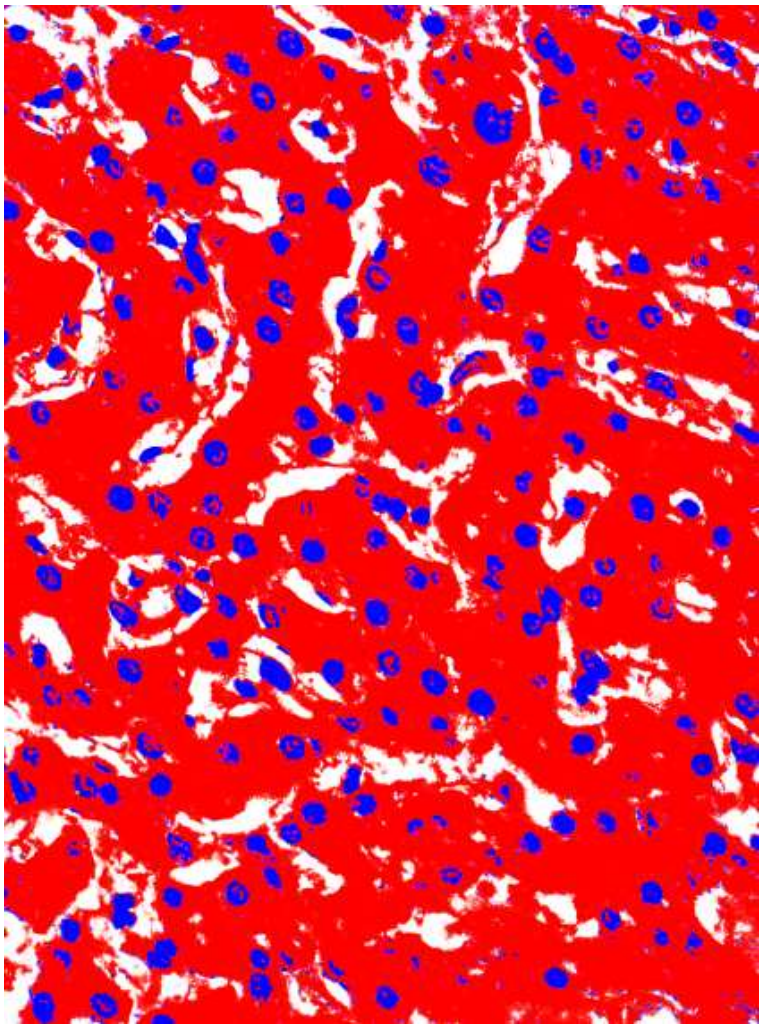

Figure 2.b

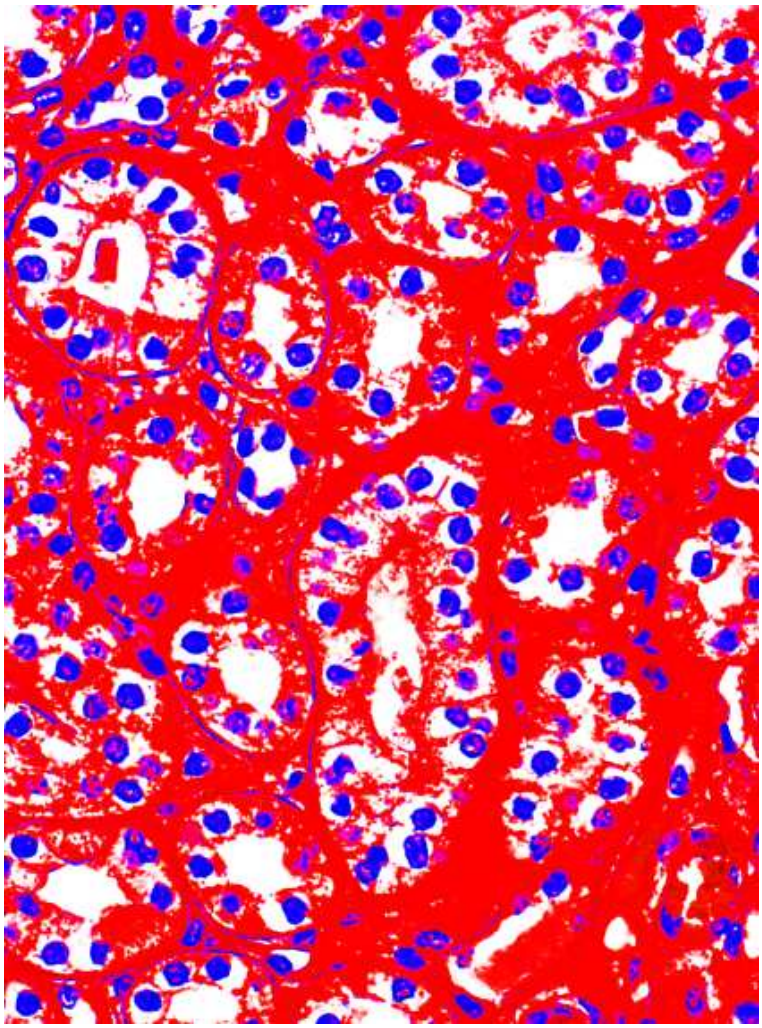

Figure 2.c

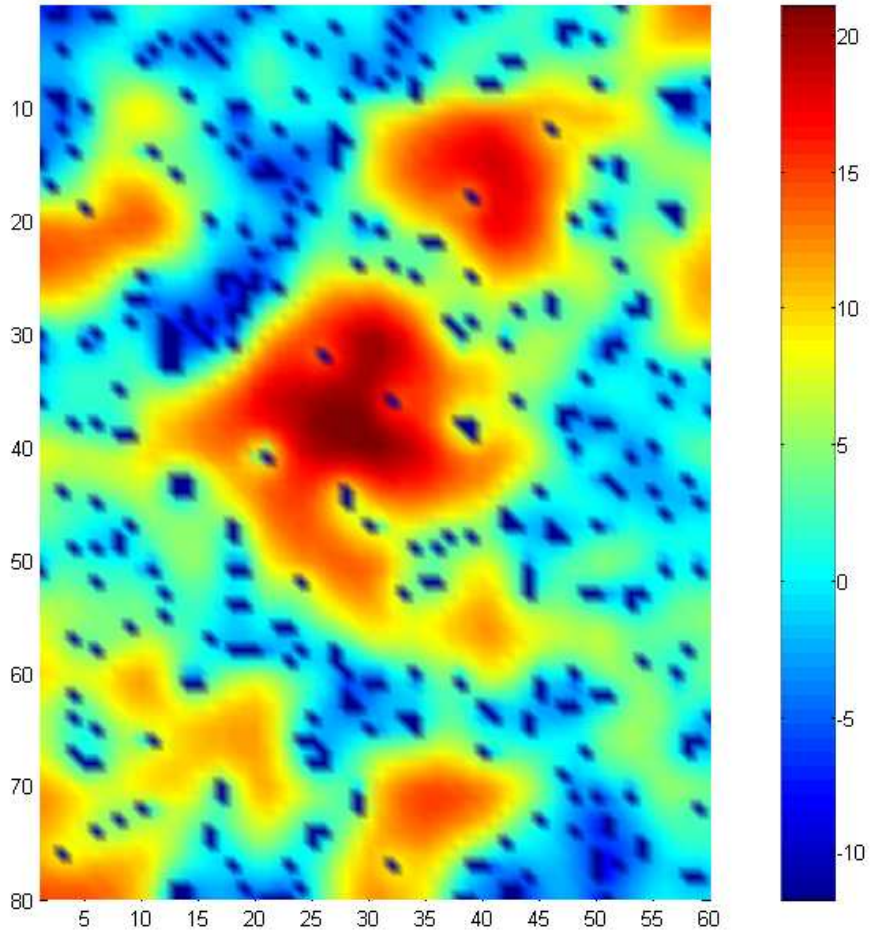
10
20
30
40
50
60
70
80
5
10
15
20
25
30
35
40
45
50
55
60
20
15
10
5
0
-5
-10

Figure 3.a

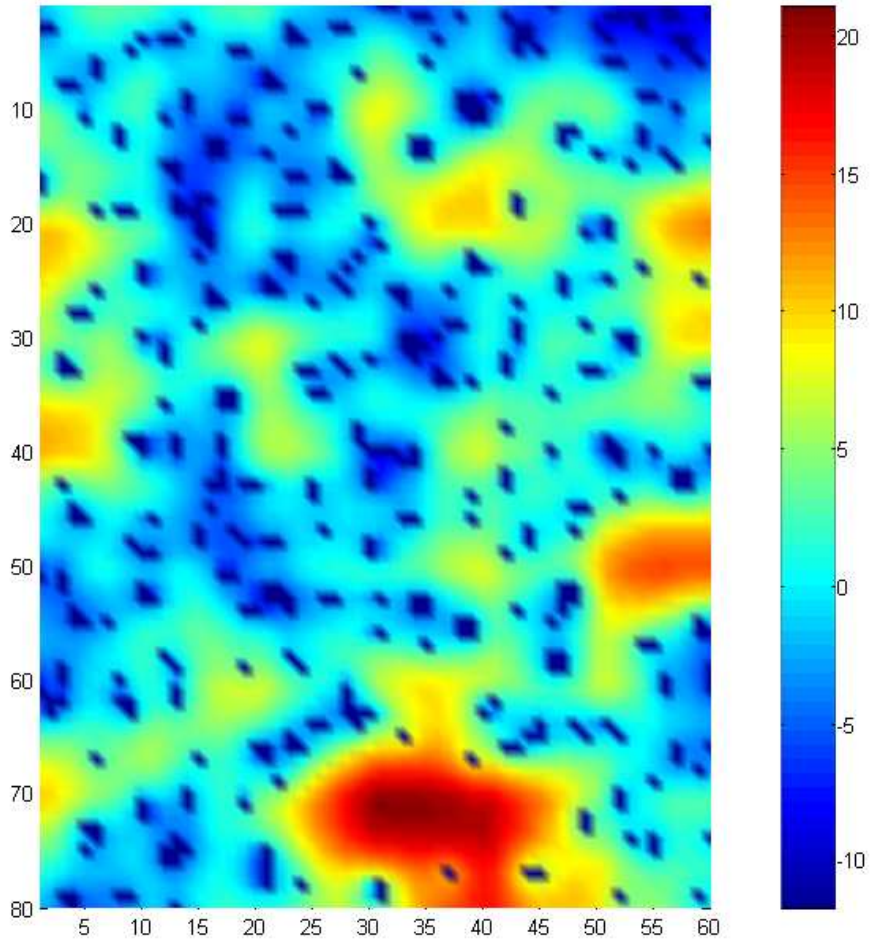
10
20
30
40
50
60
70
80
5
10
15
20
25
30
35
40
45
50
55
60
20
15
10
5
0
-5
-10

Figure 3.b

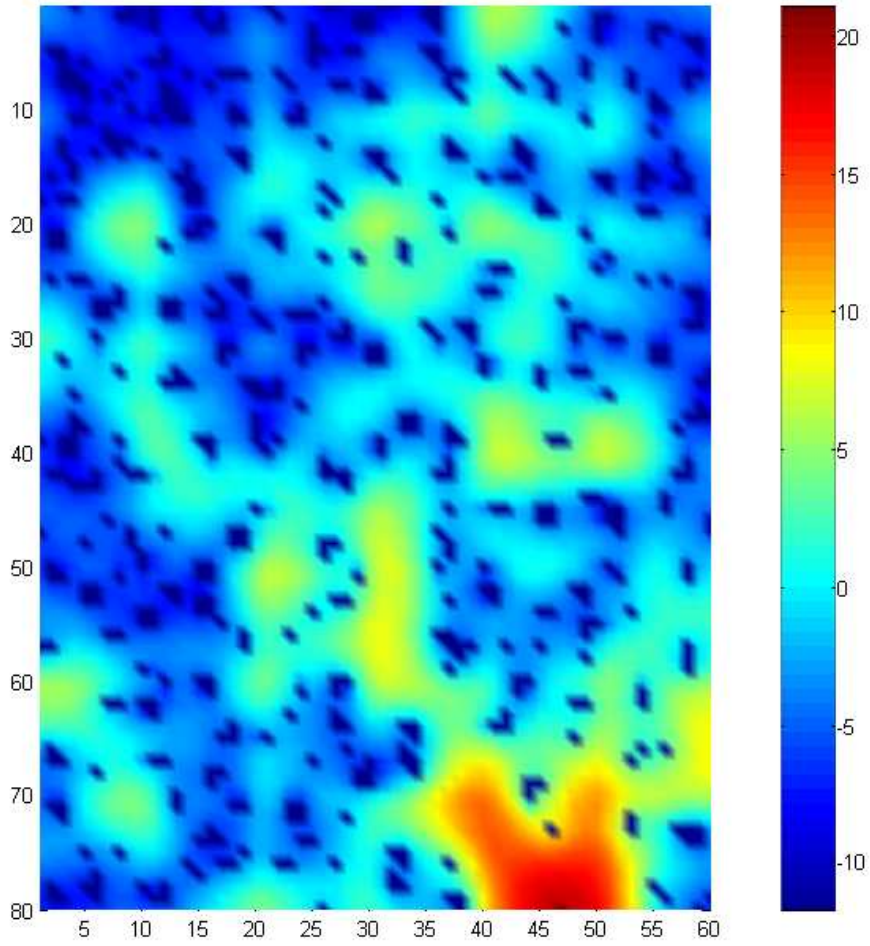
10
20
30
40
50
60
70
80
5
10
15
20
25
30
35
40
45
50
55
60
20
15
10
5
0
-5
-10

Figure 3.c

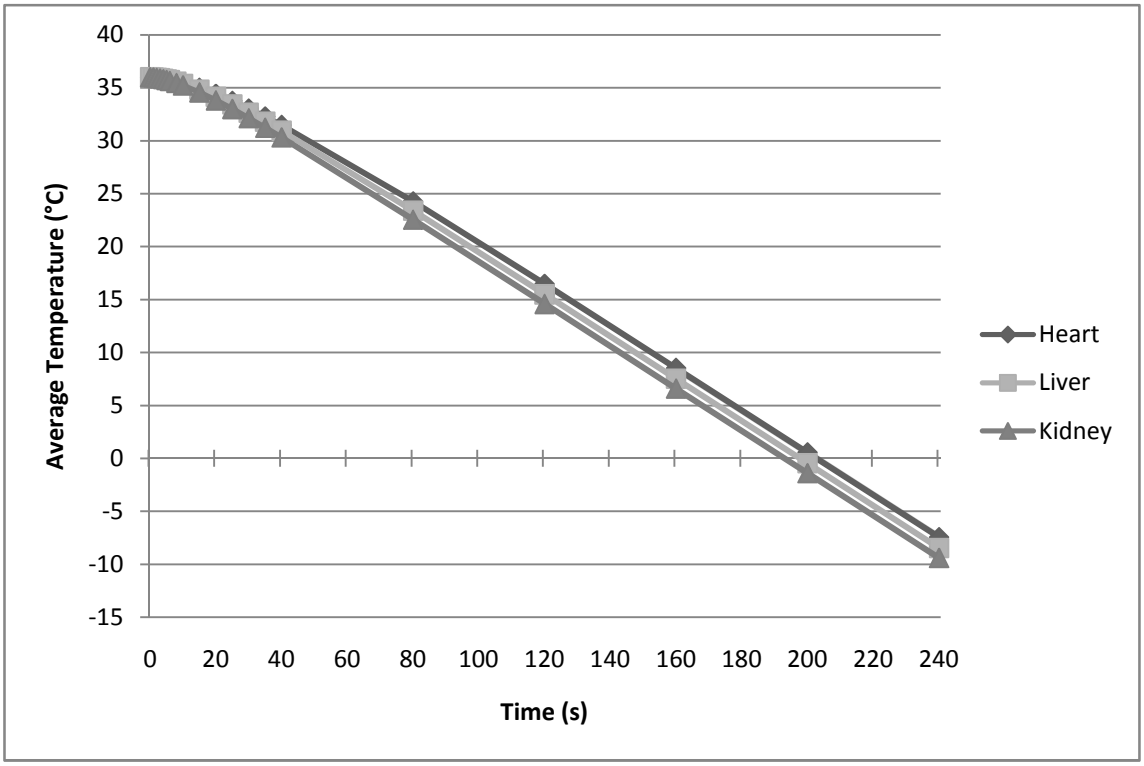
Average Temperature (°C)
40
35
30
25
20
15
10
5
0
-5
-10
-15
0
20
40
60
80
100
120
140
160
180
200
220
240
Time (s)
Heart
Liver
Kidney

Figure 4.a

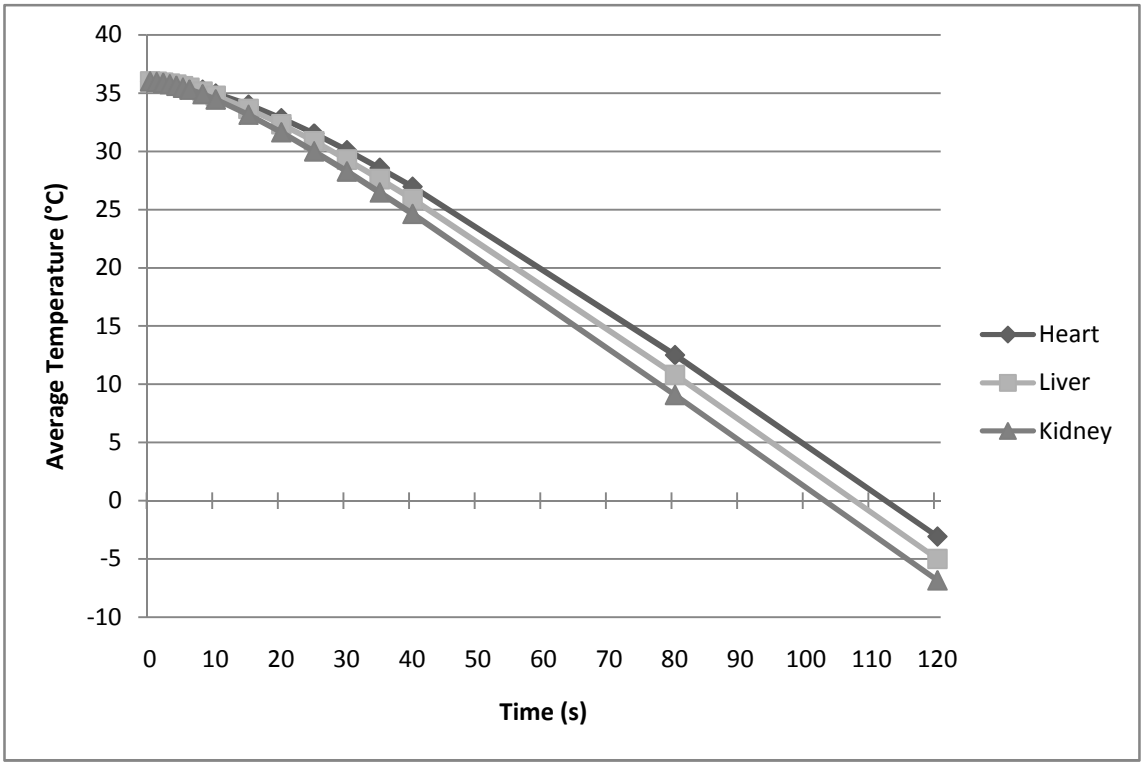
Average Temperature (°C)
40
35
30
25
20
15
10
5
0
-5
-10
0
10
20
30
40
50
60
70
80
90
100
110
120
Time (s)
Heart
Liver
Kidney

Figure 4.b

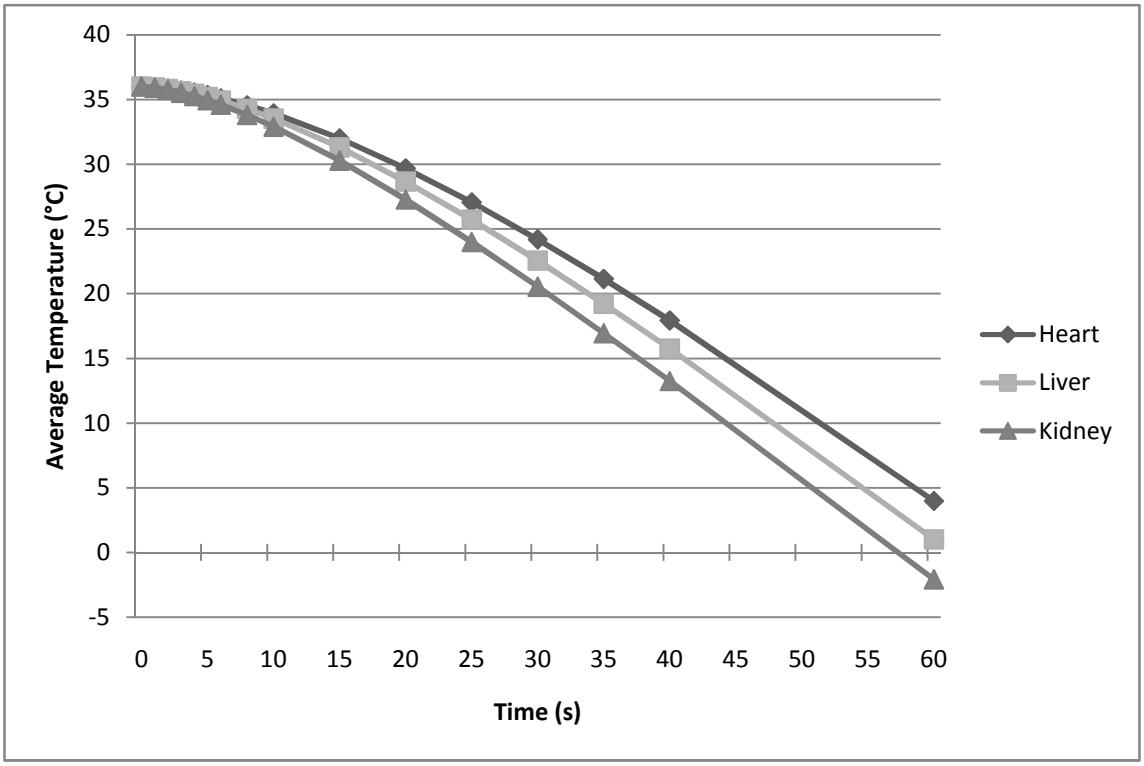
40
35
30
25
20
15
10
5
0
-5
Average Temperature (°C)
0
5
10
15
20
25
30
35
40
45
50
55
60
Time (s)
Heart
Liver
Kidney

Figure 4.c

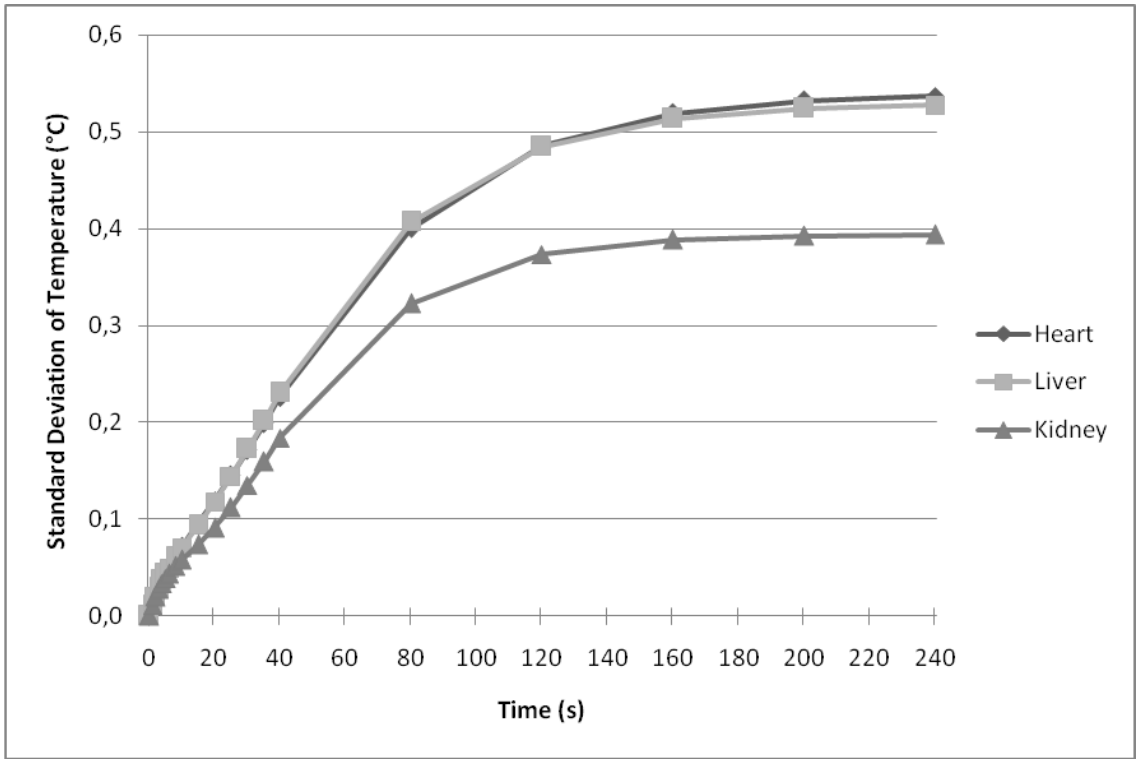
0,6
0,5
0,4
0,3
0,2
0,1
0,0
Standard Deviation of Temperature (°C)
0
20
40
60
80
100
120
140
160
180
200
220
240
Time (s)
Heart
Liver
Kidney

Figure 5.a

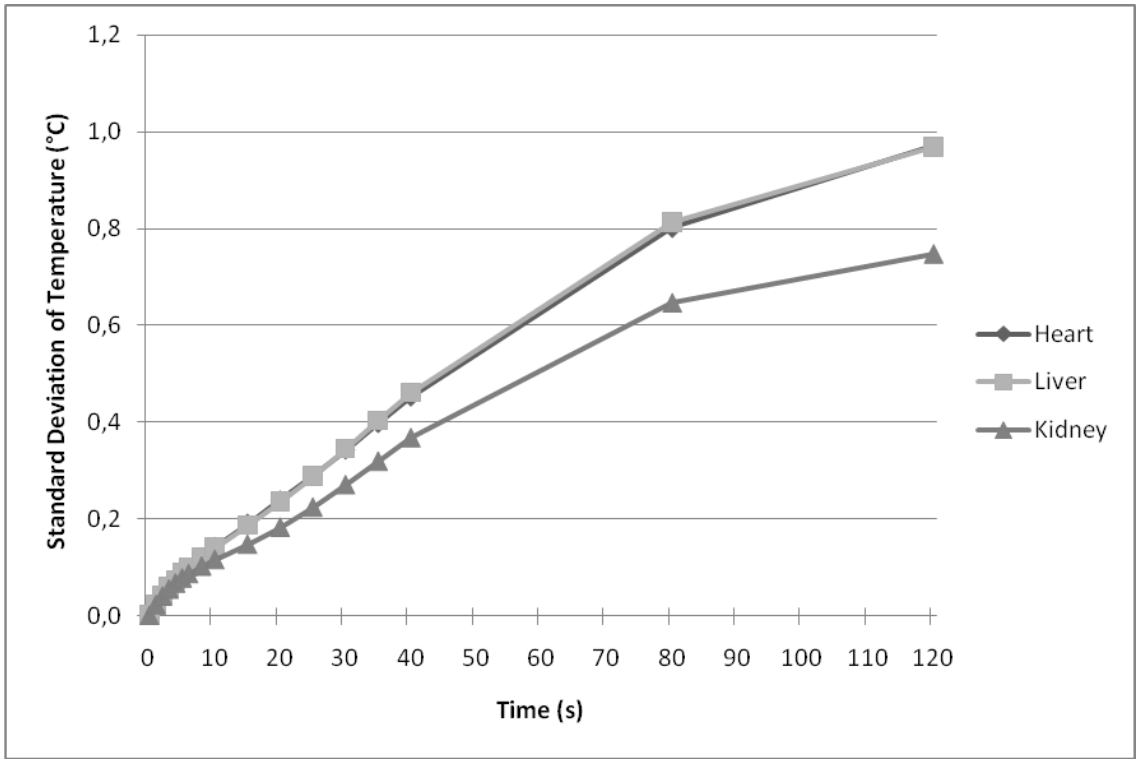
1,2
1,0
0,8
0,6
0,4
0,2
0,0
Standard Deviation of Temperature (°C)
0
10
20
30
40
50
60
70
80
90
100
110
120
Time (s)
Heart
Liver
Kidney

Figure 5.b

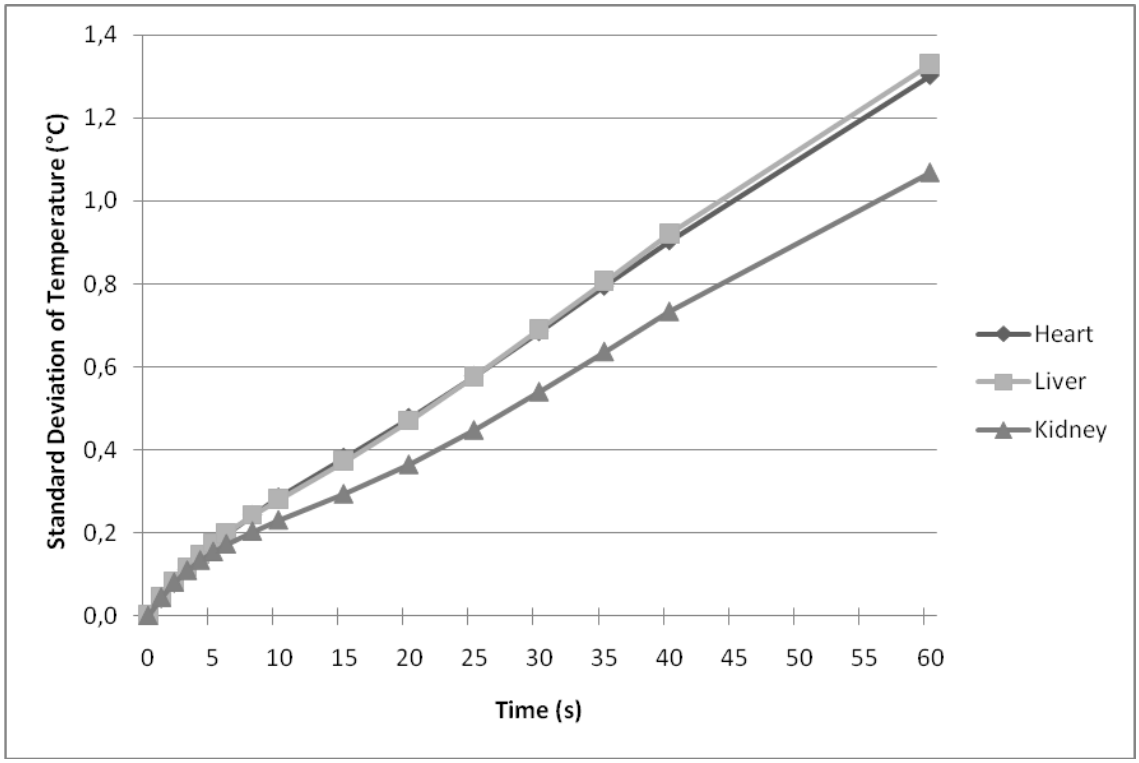
1,4
1,2
1,0
0,8
0,6
0,4
0,2
0,0
Standard Deviation of Temperature (°C)
0
5
10
15
20
25
30
35
40
45
50
55
60
Time (s)
Heart
Liver
Kidney

Figure 5.c

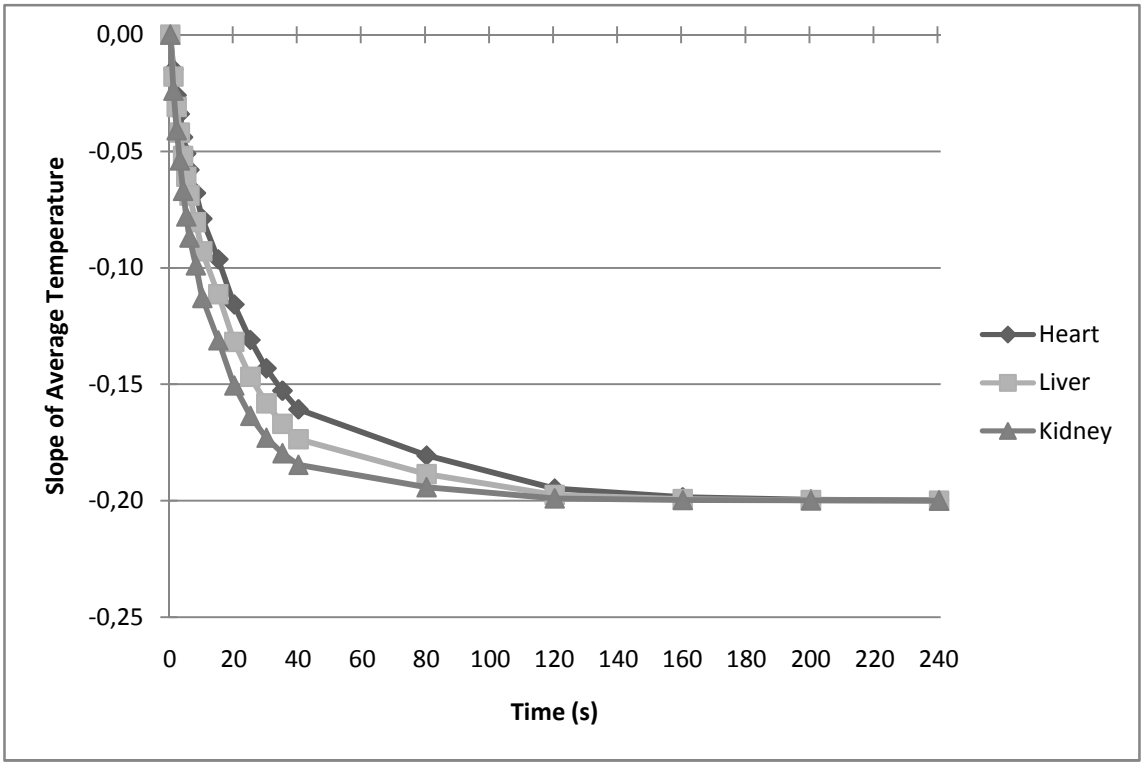
0,00
-0,05
-0,10
-0,15
-0,20
-0,25
Slope of Average Temperature
0
20
40
60
80
100
120
140
160
180
200
220
240
Time (s)
Heart
Liver
Kidney

Figure 6.a

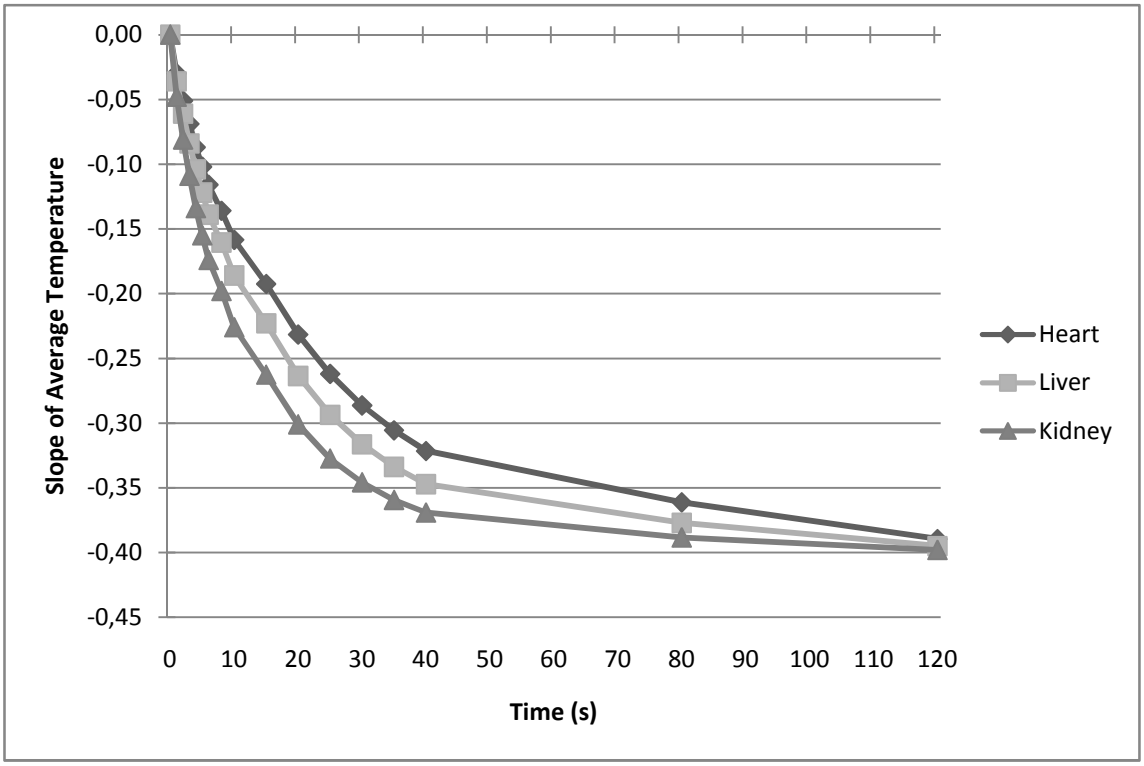
0,00
-0,05
-0,10
-0,15
-0,20
-0,25
-0,30
-0,35
-0,40
-0,45
Slope of Average Temperature
0
10
20
30
40
50
60
70
80
90
100
110
120
Time (s)
Heart
Liver
Kidney

Figure 6.b

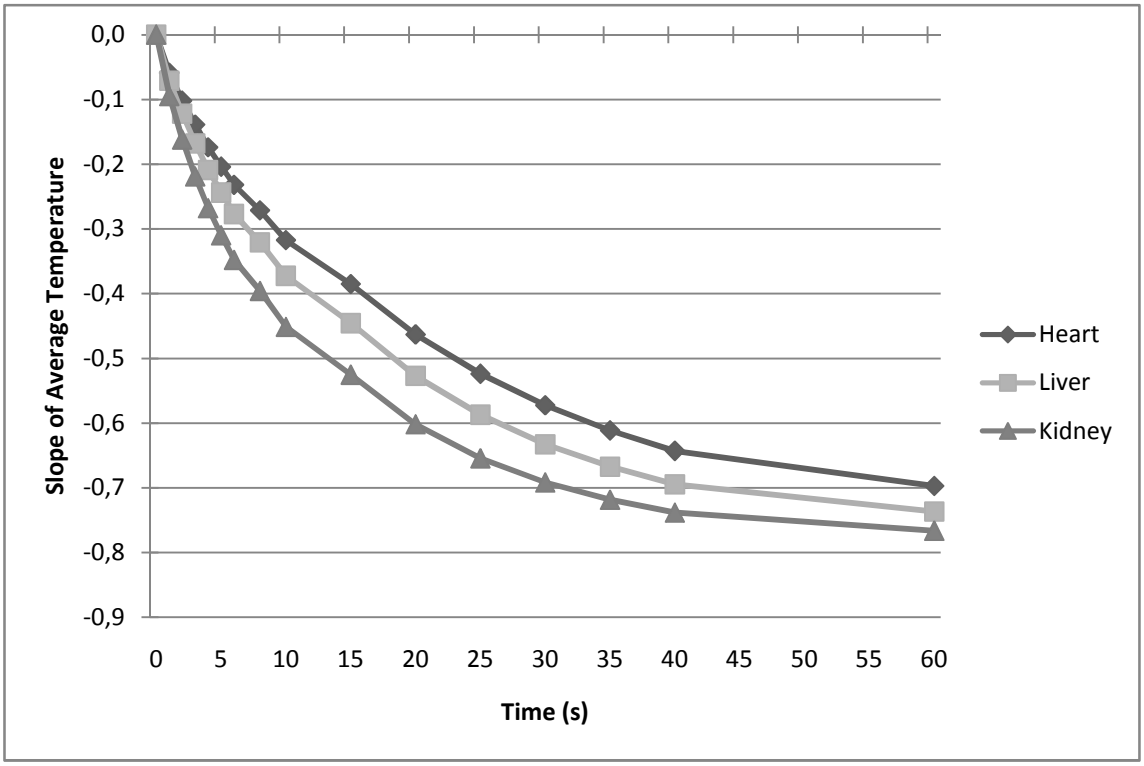
0,0
-0,1
-0,2
-0,3
-0,4
-0,5
-0,6
-0,7
-0,8
-0,9
Slope of Average Temperature
0
5
10
15
20
25
30
35
40
45
50
55
60
Time (s)
Heart
Liver
Kidney

Figure 6.c

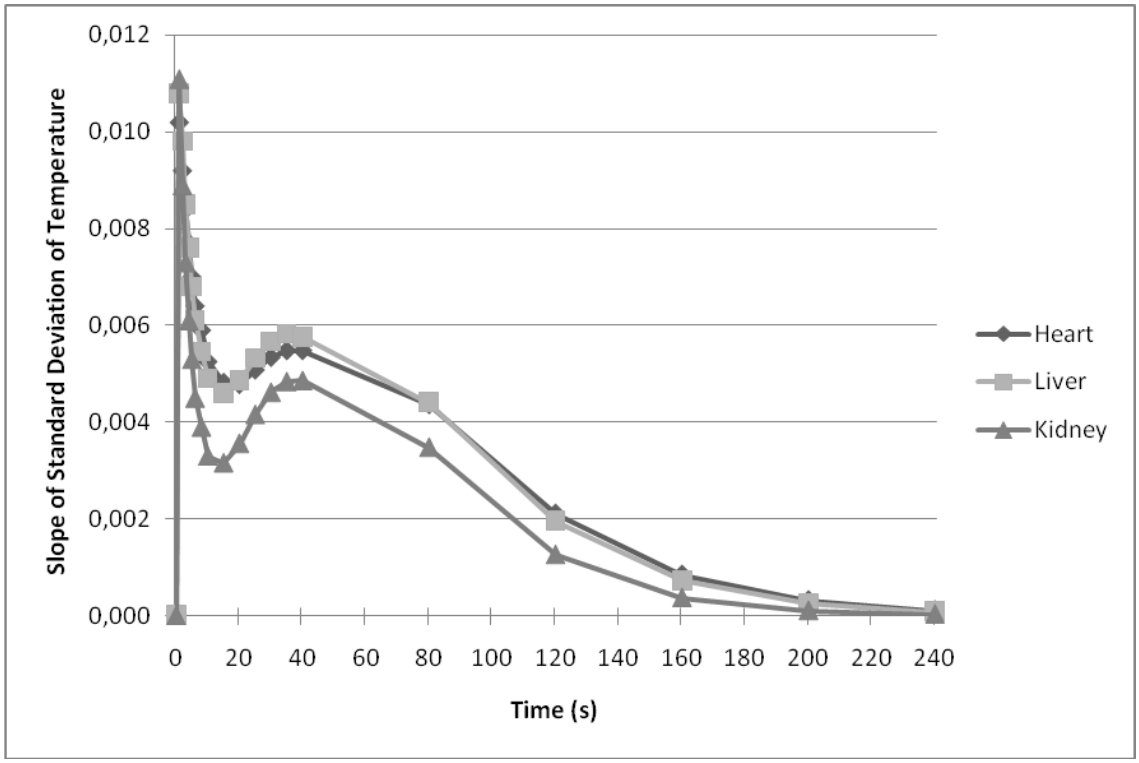
0,012
0,010
0,008
0,006
0,004
0,002
0,000
Slope of Standard Deviation of Temperature
0
20
40
60
80
100
120
140
160
180
200
220
240
Time (s)
Heart
Liver
Kidney

Figure 7.a

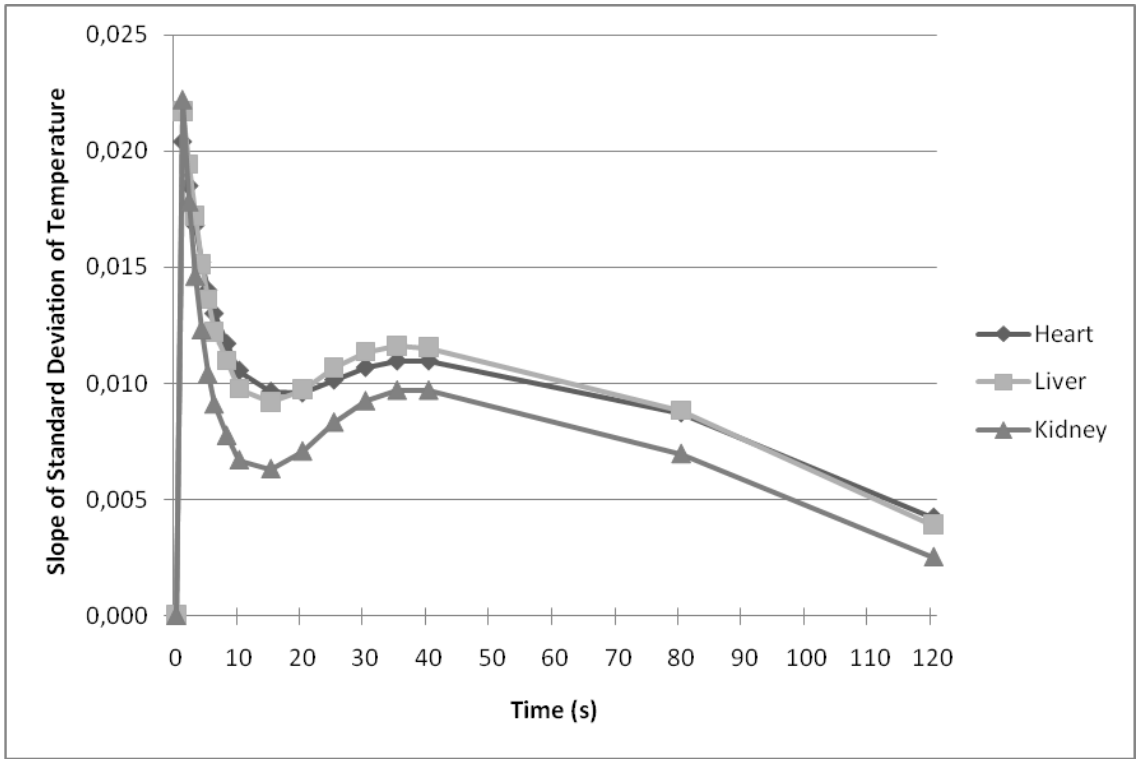
0,025
0,020
0,015
0,010
0,005
0,000
Slope of Standard Deviation of Temperature
0
10
20
30
40
50
60
70
80
90
100
110
120
Time (s)
Heart
Liver
Kidney

Figure 7.b

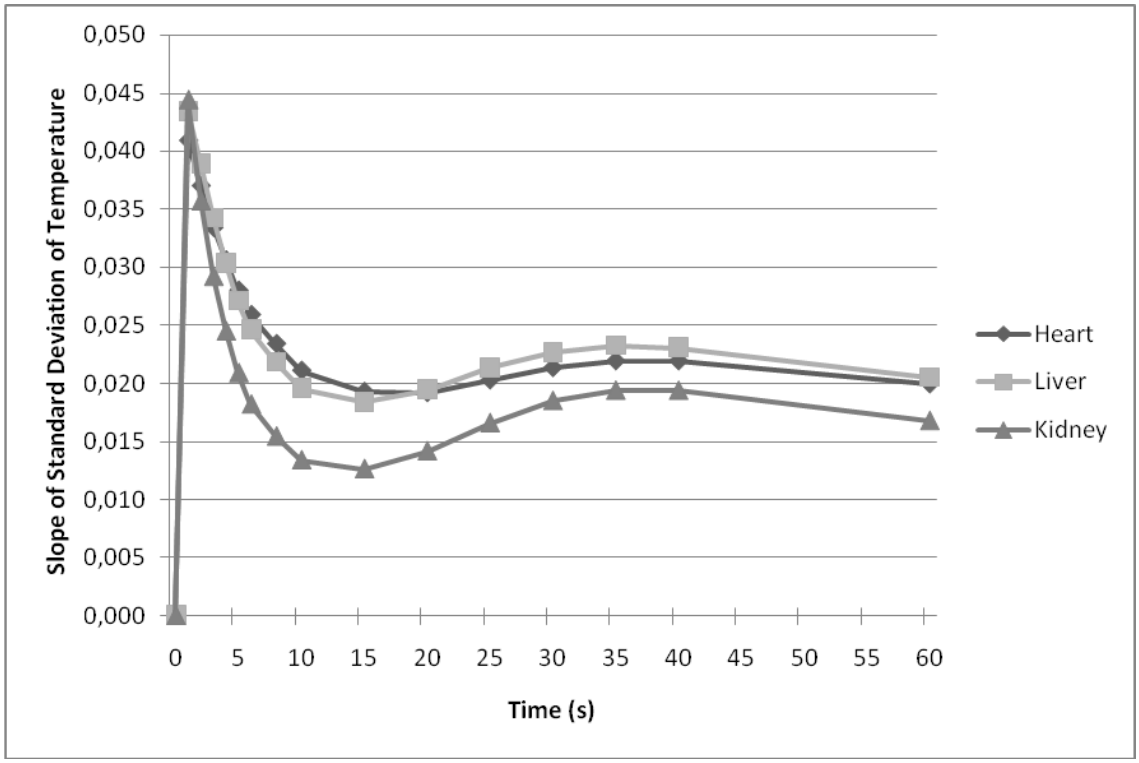
Slope of Standard Deviation of Temperature
0,050
0,045
0,040
0,035
0,030
0,025
0,020
0,015
0,010
0,005
0,000
0
5
10
15
20
25
30
35
40
45
50
55
60
Time (s)
Heart
Liver
Kidney

Figure 7.c

TABLES

Table 1: it's contained the physical properties of the materials most representative of selected organ to realize the simulations (taken from [5-7]).

Table 2: it's contained the numerical data of the average temperature for each organ during the simulated interval of time (a. -0.2º C/s: b. -0.4º C/s; -0.8º C/s).

Table 3: it's contained the numerical data of the slope of average temperature for each organ (a. -0.2º C/s: b. -0.4º C/s; -0.8º C/s).

Table 4: it's contained the numerical data of standard deviation of temperature for each organ during the simulated interval of time (a. -0.2º C/s: b. -0.4º C/s; -0.8º C/s).

Table 5: it's contained the numerical data of slope of standard deviation for each organ (a. -0.2º C/s: b. -0.4º C/s; -0.8º C/s).

	k (W/m·ºC)	ρ (kg/m^3)	c_ρ (J/kg·ºC)
Heart	0.533	1100	3712
Kidney	0.539	1022	3600
Liver	0.511	1002	3620
Connective tissue	0.570	1050	3920
Capillary / Cryoprotector	0.627	1000	4180

Table 1

Time (s)	Heart (°C)	Liver (°C)	Kidney (°C)
0	36,000	36,000	36,000
1	35,985	35,982	35,976
2	35,959	35,951	35,935
3	35,925	35,909	35,881
4	35,881	35,857	35,814
5	35,830	35,796	35,736
6	35,772	35,727	35,649
8	35,636	35,566	35,451
10	35,478	35,380	35,225
15	34,996	34,823	34,569
20	34,417	34,164	33,816
25	33,762	33,430	32,998
30	33,046	32,639	32,133
35	32,282	31,804	31,235
40	31,478	30,936	30,312
80	24,253	23,394	22,543
120	16,462	15,494	14,582
160	8,523	7,521	6,591
200	0,542	-0,470	-1,406
240	-7,451	-8,468	-9,406

Table 2.a

Time (s)	Heart (°C)	Liver (°C)	Kidney (°C)
0	36,000	36,000	36,000
1	35,970	35,964	35,952
2	35,919	35,903	35,871
3	35,850	35,819	35,762
4	35,763	35,715	35,628
5	35,661	35,593	35,473
6	35,545	35,454	35,299
8	35,273	35,133	34,903
10	34,956	34,761	34,451
15	33,993	33,646	33,138
20	32,835	32,328	31,633
25	31,525	30,860	29,996
30	30,093	29,278	28,267
35	28,565	27,609	26,470
40	26,957	25,873	24,624
80	12,507	10,788	9,087
120	-3,075	-5,011	-6,834

Table 2.b

Time (s)	Heart (°C)	Liver (°C)	Kidney (°C)
0	36,000	36,000	36,000
1	35,941	35,929	35,905
2	35,839	35,807	35,743
3	35,700	35,639	35,524
4	35,526	35,430	35,256
5	35,322	35,186	34,946
6	35,090	34,909	34,598
8	34,547	34,267	33,806
10	33,912	33,522	32,903
15	31,986	31,293	30,276
20	29,670	28,657	27,266
25	27,050	25,721	23,993
30	24,187	22,557	20,534
35	21,130	19,219	16,941
40	17,915	15,746	13,249
60	3,972	1,013	-2,080

Table 2.c

Time (s)	Heart	Liver	Kidney
0	0,0000	0,0000	0,0000
1	-0,0150	-0,0180	-0,0240
2	-0,0260	-0,0310	-0,0410
3	-0,0340	-0,0420	-0,0540
4	-0,0440	-0,0520	-0,0670
5	-0,0510	-0,0610	-0,0780
6	-0,0580	-0,0690	-0,0870
8	-0,0680	-0,0805	-0,0990
10	-0,0790	-0,0930	-0,1130
15	-0,0964	-0,1114	-0,1312
20	-0,1158	-0,1318	-0,1506
25	-0,1310	-0,1468	-0,1636
30	-0,1432	-0,1582	-0,1730
35	-0,1528	-0,1670	-0,1796
40	-0,1608	-0,1736	-0,1846
80	-0,1806	-0,1886	-0,1942
120	-0,1948	-0,1975	-0,1990
160	-0,1985	-0,1993	-0,1998
200	-0,1995	-0,1998	-0,1999
240	-0,1998	-0,2000	-0,2000

Table 3.a

Time (s)	Heart	Liver	Kidney
0	0,0000	0,0000	0,0000
1	-0,0300	-0,0360	-0,0480
2	-0,0510	-0,0610	-0,0810
3	-0,0690	-0,0840	-0,1090
4	-0,0870	-0,1040	-0,1340
5	-0,1020	-0,1220	-0,1550
6	-0,1160	-0,1390	-0,1740
8	-0,1360	-0,1605	-0,1980
10	-0,1585	-0,1860	-0,2260
15	-0,1926	-0,2230	-0,2626
20	-0,2316	-0,2636	-0,3010
25	-0,2620	-0,2936	-0,3274
30	-0,2864	-0,3164	-0,3458
35	-0,3056	-0,3338	-0,3594
40	-0,3216	-0,3472	-0,3692
80	-0,3612	-0,3771	-0,3884
120	-0,3896	-0,3950	-0,3980

Table 3.b

Time (s)	Heart	Liver	Kidney
0	0,0000	0,0000	0,0000
1	-0,0590	-0,0710	-0,0950
2	-0,1020	-0,1220	-0,1620
3	-0,1390	-0,1680	-0,2190
4	-0,1740	-0,2090	-0,2680
5	-0,2040	-0,2440	-0,3100
6	-0,2320	-0,2770	-0,3480
8	-0,2715	-0,3210	-0,3960
10	-0,3175	-0,3725	-0,4515
15	-0,3852	-0,4458	-0,5254
20	-0,4632	-0,5272	-0,6020
25	-0,5240	-0,5872	-0,6546
30	-0,5726	-0,6328	-0,6918
35	-0,6114	-0,6676	-0,7186
40	-0,6430	-0,6946	-0,7384
60	-0,6972	-0,7367	-0,7665

Table 3.c

Time (s)	Heart (°C)	Liver (°C)	Kidney (°C)
0	0,0000	0,0000	0,0000
1	0,0102	0,0108	0,0111
2	0,0194	0,0206	0,0200
3	0,0278	0,0291	0,0273
4	0,0355	0,0367	0,0334
5	0,0425	0,0435	0,0387
6	0,0489	0,0496	0,0432
8	0,0607	0,0605	0,0510
10	0,0712	0,0703	0,0576
15	0,0953	0,0933	0,0734
20	0,1192	0,1176	0,0912
25	0,1446	0,1442	0,1120
30	0,1713	0,1725	0,1351
35	0,1987	0,2016	0,1593
40	0,2261	0,2304	0,1836
80	0,4006	0,4066	0,3229
120	0,4851	0,4849	0,3735
160	0,5191	0,5139	0,3884
200	0,5319	0,5240	0,3926
240	0,5365	0,5274	0,3938

Table 4.a

Time (s)	Heart (°C)	Liver (°C)	Kidney (°C)
0	0,0000	0,0000	0,0000
1	0,0204	0,0217	0,0222
2	0,0389	0,0411	0,0400
3	0,0557	0,0583	0,0546
4	0,0709	0,0734	0,0669
5	0,0849	0,0870	0,0773
6	0,0979	0,0992	0,0864
8	0,1213	0,1211	0,1019
10	0,1424	0,1406	0,1153
15	0,1906	0,1865	0,1469
20	0,2385	0,2351	0,1823
25	0,2892	0,2884	0,2239
30	0,3426	0,3451	0,2701
35	0,3974	0,4031	0,3186
40	0,4522	0,4607	0,3671
80	0,8013	0,8132	0,6458
120	0,9702	0,9697	0,7468

Table 4.b

Time (s)	Heart (°C)	Liver (°C)	Kidney (°C)
0	0,0000	0,0000	0,0000
1	0,0409	0,0434	0,0444
2	0,0779	0,0823	0,0801
3	0,1113	0,1165	0,1093
4	0,1419	0,1468	0,1338
5	0,1699	0,1739	0,1547
6	0,1958	0,1985	0,1729
8	0,2426	0,2421	0,2038
10	0,2848	0,2812	0,2306
15	0,3812	0,3731	0,2938
20	0,4771	0,4702	0,3647
25	0,5785	0,5768	0,4477
30	0,6852	0,6901	0,5402
35	0,7948	0,8062	0,6372
40	0,9044	0,9214	0,7341
60	1,3031	1,3309	1,0698

Table 4.c

Time (s)	Heart	Liver	Kidney
0	0,0000	0,0000	0,0000
1	0,0102	0,0108	0,0111
2	0,0092	0,0098	0,0089
3	0,0084	0,0085	0,0073
4	0,0077	0,0076	0,0061
5	0,0070	0,0068	0,0053
6	0,0064	0,0061	0,0045
8	0,0059	0,0055	0,0039
10	0,0053	0,0049	0,0033
15	0,0048	0,0046	0,0032
20	0,0048	0,0049	0,0036
25	0,0051	0,0053	0,0042
30	0,0053	0,0057	0,0046
35	0,0055	0,0058	0,0048
40	0,0055	0,0058	0,0049
80	0,0044	0,0044	0,0035
120	0,0021	0,0020	0,0013
160	0,0009	0,0007	0,0004
200	0,0003	0,0003	0,0001
240	0,0001	0,0001	0,0000

Table 5.a

Time (s)	Heart	Liver	Kidney
0	0,0000	0,0000	0,0000
1	0,0204	0,0217	0,0222
2	0,0185	0,0194	0,0178
3	0,0168	0,0172	0,0146
4	0,0152	0,0151	0,0123
5	0,0140	0,0136	0,0104
6	0,0130	0,0122	0,0091
8	0,0117	0,0110	0,0078
10	0,0106	0,0098	0,0067
15	0,0096	0,0092	0,0063
20	0,0096	0,0097	0,0071
25	0,0101	0,0107	0,0083
30	0,0107	0,0113	0,0092
35	0,0110	0,0116	0,0097
40	0,0110	0,0115	0,0097
80	0,0087	0,0088	0,0070
120	0,0042	0,0039	0,0025

Table 5.b

Time (s)	Heart	Liver	Kidney
0	0,0000	0,0000	0,0000
1	0,0409	0,0434	0,0444
2	0,0370	0,0389	0,0357
3	0,0334	0,0342	0,0292
4	0,0306	0,0303	0,0245
5	0,0280	0,0271	0,0209
6	0,0259	0,0246	0,0182
8	0,0234	0,0218	0,0155
10	0,0211	0,0196	0,0134
15	0,0193	0,0184	0,0126
20	0,0192	0,0194	0,0142
25	0,0203	0,0213	0,0166
30	0,0213	0,0227	0,0185
35	0,0219	0,0232	0,0194
40	0,0219	0,0230	0,0194
60	0,0199	0,0205	0,0168

Table 5.c